technologies

MDPI

Communication

Self-Powered Electrochemical Humidity Sensor Based on Hydroxylated Multi-Walled Carbon Nanotubes-Modified CeO_2 Nanoparticles

Zhen Yuan, Chong Tan, Zaihua Duan *, Yadong Jiang and Huiling Tai *

State Key Laboratory of Electronic Thin Films and Integrated Devices, School of Optoelectronic Science and Engineering, University of Electronic Science and Technology of China (UESTC), Chengdu 611731, China
* Correspondence: zaihuaduan@uestc.edu.cn (Z.D.); taitai1980@uestc.edu.cn (H.T.)

Abstract

Electrochemical humidity (ECH) sensors with self-generating capability have attracted widespread attention. In this work, a self-powered ECH sensor is developed using hydroxylated multi-walled carbon nanotubes (OH-MWCNTs)-modified CeO_2 nanoparticles as the humidity sensing materials. The results show that the OH-MWCNTs are beneficial for improving the humidity sensing performances of the CeO_2 nanoparticles. The optimized OH-MWCNTs/CeO_2 ECH sensor exhibits a wide detection range (0–91.5% relative humidity (RH)) and fast response and recovery times (18.6 and 6.9 s), attributed to the synergistic effect of OH-MWCNTs and CeO_2 nanoparticles. In addition, a single OH-MWCNTs/CeO_2 ECH sensor can output a voltage of 0.711 V and a load power of 0.376 μW at 91.5% RH. When applied for respiratory rate monitoring, the OH-MWCNTs/CeO_2 ECH sensor can accurately detect respiratory rate by converting exhaled humidity into voltage signal. This work demonstrates that the OH-MWCNTs-modified oxide material of CeO_2 nanoparticles is a good candidate for fabricating self-powered ECH sensor.

Keywords: humidity sensor; hydroxylated multi-walled carbon nanotubes; CeO_2; electrochemical reaction; respiratory rate detection

check for updates

Academic Editors: Silvia Rizzato and Antonino Proto

Received: 15 September 2025
Revised: 8 October 2025
Accepted: 13 October 2025
Published: 15 October 2025

Citation: Yuan, Z.; Tan, C.; Duan, Z.; Jiang, Y.; Tai, H. Self-Powered Electrochemical Humidity Sensor Based on Hydroxylated Multi-Walled Carbon Nanotubes-Modified CeO_2 Nanoparticles. *Technologies* **2025**, *13*, 467. https://doi.org/10.3390/technologies13100467

Copyright: © 2025 by the authors. Licensee MDPI, Basel, Switzerland. This article is an open access article distributed under the terms and conditions of the Creative Commons Attribution (CC BY) license (https://creativecommons.org/licenses/by/4.0/).

1. Introduction

Humidity sensors have many applications, such as environmental monitoring, industrial control, smart homes, and emerging respiratory status detection [1–7]. Traditional humidity sensors mainly convert humidity into capacitance, impedance, resistance, and optical and frequency signals [1], and the acquisition of these signals requires power consumption due to external voltage. In recent years, the self-powered electrochemical humidity (ECH) sensors have emerged as a promising alternative that can directly output voltage signal [8–29]. Therefore, researchers have conducted extensive research on the device structure (mainly based on electrode coplanar structure), electrode materials (mainly composed of metal foils with different redox activities, such as Cu positive electrode and Al, Zn, and Mg negative electrode), and humidity-sensing materials [8–29]. Specifically, the humidity-sensing materials are closely related to the performances of the ECH sensors and have received significant attention.

ECH sensors rely on adsorbed water molecules and electrochemical reactions, so humidity-sensing materials need to have both good hydrophilicity and ion/proton conductivity. So far, the reported ECH sensors usually use two-dimensional materials (such as

graphene oxide, $Ti_3C_2T_x$, and WS_2) [8,11,12,19,26], polymer materials (such as hyaluronic, polyvinyl alcohol (PVA), and polydopamine (PDA)) [16,19], cellulose/paper [9,18,20], and salt electrolytes (such as NaCl, LiCl, KCl, MgCl, and LiBr) [9,10,13–17,19–27]. In addition, to reduce the internal resistance of ECH sensors and increase power generation, the conductive materials such as carbon nanotubes and carbon black can be added to humidity-sensing materials [14,16,20]. It is not difficult to find that two-dimensional materials, polymer materials, and cellulose/paper are all good hydrophilic materials and are also commonly used for fabricating other types of humidity sensors. However, these humidity-sensitive materials have a stability issue. For other types of humidity sensors, the oxides with good stability are important humidity-sensing materials [30]. As far as we know, the oxides have not yet received important attention and development in ECH sensors. The possible reason is that the hydrophilicity and ion/proton conductivity of most oxides are relatively poor compared to other humidity-sensing materials, which poses challenges to fabricate ECH sensors. Among various traditional humidity-sensing oxide materials (such as ZnO [31,32], SnO_2 [33,34], TiO_2 [35,36], Co_3O_4 [37–39], and CeO_2 [40–48]), CeO_2 has mixed Ce valence states (Ce^{4+} and Ce^{3+}) and abundant oxygen vacancies, resulting in relatively good water molecule adsorption capacity and ion conductivity, and is therefore used to fabricate resistive and capacitive humidity sensors [40–48]. Based on these characteristics, it is predicted that CeO_2 can be used as a candidate for fabricating ECH sensors. To reduce the resistance of CeO_2, materials with good conductivity, such as carbon materials, can be combined [49–53]. In addition, to further enhance the hydrophilicity of CeO_2, the hydrophilic and conductive material, such as hydroxylated multi-walled carbon nanotubes (OH-MWCNTs), can be selected for modifying CeO_2.

Based on the above discussion and analysis, in this work, we aim to develop the application of oxide materials in the field of ECH sensors. Specifically, we construct an ECH sensor using OH-MWCNTs/CeO_2 as humidity-sensing materials and Cu/Zn as electrodes. The resulting ECH sensor exhibits wide humidity detection range and rapid response/recovery speed. In addition, we demonstrate the application of ECH sensor in respiratory rate detection.

2. Experimental Section

2.1. Materials

The main materials for fabricating OH-MWCNTs/CeO_2 ECH sensor include OH-MWCNTs powder (diameter: ~12 nm; Shenzhen Guosen Pilot Technology Co., Ltd., Shenzhen, China), CeO_2 nanoparticles dispersion liquid (diameter: 30~50 nm; 20 wt% in water; Shanghai D&B Biological Science and Technology Co., Ltd., Shanghai, China), Al_2O_3 ceramic substrate (size: 10 mm × 10 mm, Taizhou Jingwei Special Ceramics Co., Ltd., Taizhou, China), and Cu/Zn foil tapes (thickness: ~65 μm, Shenzhen Mileqi Tape Co., Ltd., Shenzhen, China).

2.2. Fabrication and Characterization

In order to investigate the effect of different proportions of OH-MWCNTs on humidity-sensing performance, the amount of CeO_2 is fixed. The manufacturing processes of OH-MWCNTs/CeO_2 humidity-sensing materials and corresponding ECH sensors are as follows: Firstly, 20 wt% CeO_2 aqueous dispersion liquid was diluted to 4 wt% CeO_2 aqueous dispersion liquid using deionized water. Specifically, 2 mL CeO_2 aqueous dispersion liquid (20 wt%) was mixed with 8 mL deionized water to obtain 10 mL CeO_2 aqueous dispersion liquid (4 wt%). Secondly, 1, 2, 3, and 4 mg OH-MWCNTs powders were added to 1 mL of 4 wt% CeO_2 aqueous dispersion to prepare OH-MWCNTs/CeO_2 humidity-sensing materials, labeled as #1, #2, #3, and #4, respectively. Thirdly, Cu and Zn foil tapes were pasted onto

the Al_2O_3 ceramic substrate with a gap of 0.5 mm between the two electrodes, referring to our previous studies [9]. Fourthly, the OH-MWCNTs/CeO_2 humidity-sensing materials were uniformly coated on the gap between the electrodes using a brush to obtain #1, #2, #3, and #4 ECH sensors (thickness: ~40 μm [11]). Finally, the OH-MWCNTs/CeO_2 ECH sensors were prepared by drying at 60 °C for 10 min. For comparative analysis, the CeO_2 ECH sensor and OH-MWCNTs ECH sensor were prepared using the same method, labeled as #5 and #6, respectively. Batch consistency is important for evaluating the performance of sensors. It should be noted that the ECH sensor preparation process involves many manual steps, making it difficult to ensure process consistency. Therefore, we did not investigate the batch consistency of ECH sensors.

The morphologies and elements distribution of the OH-MWCNTs/CeO_2 materials and optimized ECH sensor were characterized by field emission scanning electron microscopy (FE-SEM, Carl Zeiss, GeminiSEM 300, Oberkochen, Germany) with an energy-dispersive spectrometer (EDS, Oxford Instruments, Ultim Max, Oxford, UK) and transmission electron microscopy (TEM, JEOL, JEM-2100 Plus, Tokyo, Japan). The dynamic contact angles of the CeO_2 and OH-MWCNTs/CeO_2 humidity-sensing films were recorded by a contact angle tester (Dataphysics OCA20, Filderstadt, Germany). The crystal structure and elements of the CeO_2 and OH-MWCNTs/CeO_2 were analyzed by X-ray diffraction (XRD, Bruker D8 ADVANCE, Cu Kα1 irradiation source, λ = 0.15406 nm) and X-ray photoelectron spectroscopy (XPS, Thermo Fisher Scientific, K-Alpha spectrometer, Waltham, MA, USA). It should be noted that the characterizations of the OH-MWCNTs/CeO_2 composite materials are only based on the optimal sample #2 according to the subsequent humidity-sensing performances.

2.3. Performance Testing

For the humidity sensing and power generation performance testing of ECH sensors, we have provided a detailed description in our previous research, combined with a testing schematic diagram [9–11,54]. Therefore, we only briefly describe it as follows: Firstly, different calibrated relative humidities (RHs) were obtained through the bubble method, including 0%, 18.7%, 28.8%, 41.1%, 51.9%, 60.8%, 72.0%, 79.3%, 86.7%, and 91.5% RH. Secondly, the spontaneous output voltage of the ECH sensor at different RHs was recorded through a digital multimeter (DMM 6500, Keithley, Cleveland, OH, USA). The response and recovery times of the ECH sensor are defined as the time it takes for the output voltage to reach 90% change during the adsorption and desorption processes of water molecules under 91.5% RH [1–3].

3. Results and Discussion

3.1. Characterization

Figure 1a shows the schematic diagram of the ECH sensor, consisting of OH-MWCNTs/CeO_2 humidity-sensing material, Cu/Zn electrodes, and Al_2O_3 ceramic substrate. Correspondingly, the surface SEM image in Figure 1b confirms the device structure of the ECH sensor. Figure 1c shows the high magnification SEM image of the OH-MWCNTs/CeO_2 film, with OH-MWCNTs and CeO_2 nanoparticles forming a rough surface structure. The EDS mappings of the OH-MWCNTs/CeO_2 ECH sensor further indicate the humidity-sensing material and electrode compositions of the Zn, C, O, Ce, and Cu elements (Figure 1d).

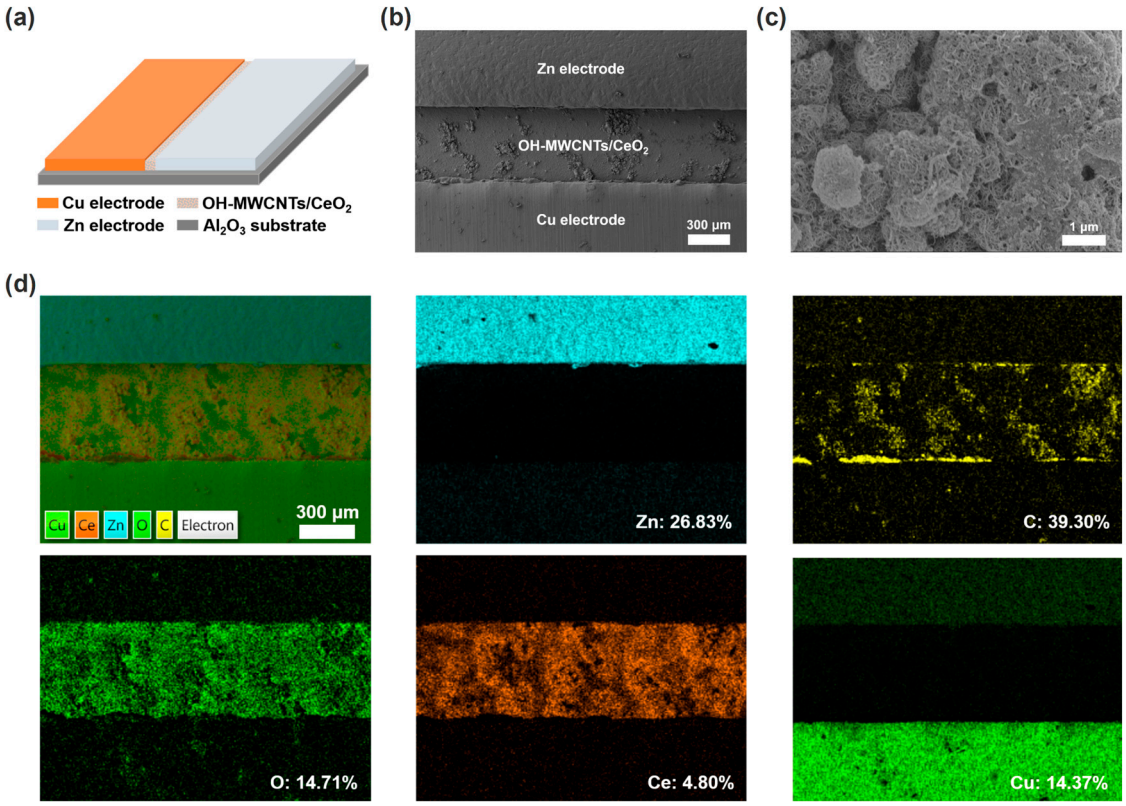


Figure 1. (**a**) Schematic diagram of the OH-MWCNTs/CeO_2 ECH sensor. (**b**) Surface SEM image of the OH-MWCNTs/CeO_2 ECH sensor. (**c**) High-magnification SEM image of the OH-MWCNTs/CeO_2 film. (**d**) EDS mappings of the OH-MWCNTs/CeO_2 ECH sensor and corresponding Zn, C, O, Ce, and Cu elements.

Figure 2a shows the XRD patterns of OH-MWCNTs/CeO_2, with eight distinct diffraction peaks corresponding to the (111), (200), (220), (311), (222), (400), (331), and (420) crystal planes of the CeO_2 (JCPDS Card No. 34–0394) [41,46]. It should be noted that, due to the large proportion of CeO_2 nanoparticles and strong diffraction peaks in the crystal structures, the diffraction peaks of OH-MWCNTs are suppressed, with only a weak (002) crystal plane [55,56]. As shown in Figure 2b, OH-MWCNTs and CeO_2 nanoparticles are combined together. Figure S1 shows the XPS fully scanned spectra of the OH-MWCNTs, CeO_2, and OH-MWCNTs/CeO_2, further confirming the elemental composition of each material. The oxygen element in the material is mainly composed of adsorbed water molecules, hydroxyl group (-OH), and lattice oxygen, among which water molecules and -OH are conducive to the adsorption of water molecules [57]. Figure 2c–e show the O 1s high-resolution spectra of the OH-MWCNTs/CeO_2, CeO_2, and OH-MWCNTs. Peaks 1, 2, and 3 correspond to adsorbed water molecules, -OH, and lattice oxygen, respectively. It can be seen that there is basically no lattice oxygen in OH-MWCNTs (Figure 2e). After calculation, adsorbed water molecules and -OH in OH-MWCNTs/CeO_2 account for 51.1%, larger than CeO_2 (45.3%), due to the introduction of hydrophilic OH-MWCNTs. Therefore, OH-MWCNTs/CeO_2 is expected to have better humidity-sensing performances than CeO_2 [57]. It should be noted that OH-MWCNTs has excellent conductivity and is prone to short circuits, so it cannot be directly used for fabricating ECH sensor. In order to visually demonstrate the hydrophilicity of the humidity-sensing films, Figure 2f shows the contact angles of CeO_2 and OH-MWCNTs/CeO_2 films, both of which have contact angles less than 90° and exhibit good hydrophilicity [54]. Obviously, due to the introduction of hydrophilic OH-MWCNTs, the OH-MWCNTs/CeO_2 film exhibits a smaller contact angle and is more hydrophilic than CeO_2 film.

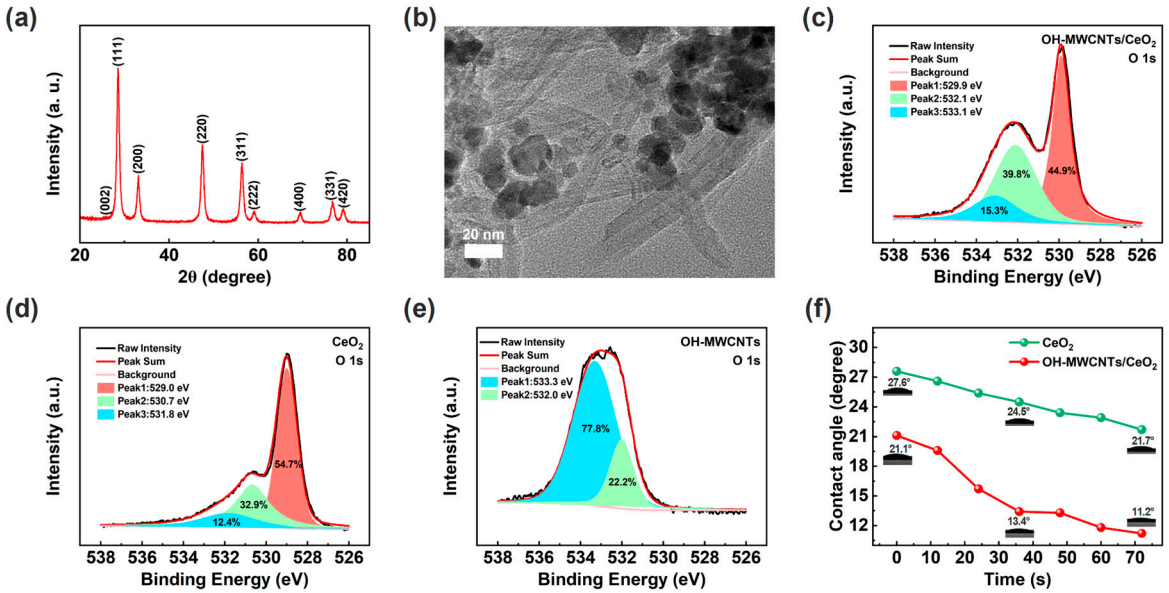


Figure 2. (**a**) XRD patterns of the OH-MWCNTs/CeO_2. (**b**) TEM image of the OH-MWCNTs/CeO_2. (**c**) O 1 s of the OH-MWCNTs/CeO_2. (**d**) O 1 s of the CeO_2. (**e**) O 1 s of the OH-MWCNTs. (**f**) Dynamic contact angles of the CeO_2 and OH-MWCNTs/CeO_2 humidity-sensing films.

3.2. Performances

In order to optimize the load ratio of OH-MWCNTs on CeO_2, the response curves of the different ECH sensors (#1–6) under 91.5% RH were tested as shown in Figure 3a. In terms of response voltage, the OH-MWCNTs/CeO_2 (#1–4) and CeO_2 (#5) ECH sensors are significantly greater than OH-MWCNTs ECH sensor (#6), with #2 ECH sensor having the highest response voltage of about 0.711 V (Figure 3b). The #6 ECH sensor has almost no response voltage due to short circuit caused by the excellent conductivity of OH-MWCNTs. Response and recovery times are important parameters of a humidity sensor, so further comparison of response and recovery time is shown in Figure 3c. The response and recovery times of humidity sensor are usually opposite and are influenced by various factors such as the hydrophilicity of the material and the response value of the humidity sensor. In terms of experimental results, the #2 ECH sensor balances fast response and recovery speed. Therefore, the #2 ECH sensor is used as the optimized sensor for subsequent testing and application demonstrations. Figure 3d shows the response curve of the optimized ECH sensor under different RHs, indicating a wide detection range of 0–91.5% RH. The magnified response and recovery curve in Figure 3e shows that the response and recovery times are 18.6 s and 6.9 s. It should be noted that there are some data points in the response and recovery curves that are not very smooth, which may be caused by the unstable airflow generated by the bubble method and the switching of different RH levels. Figure 3f shows 10 repetitive responses with a small relative standard deviation (RSD) of 1.33%, indicating a good repeatability. Figure 3g shows the response curve during water molecule adsorption and desorption processes. As the humidity increases, the response voltage of the ECH sensor gradually increases. Conversely, when the humidity gradually decreases, the response voltage of the ECH sensor gradually decreases, forming a humidity hysteresis phenomenon. Correspondingly, according to the humidity hysteresis curves in Figure 3h, the humidity hysteresis of the ECH sensor is about 5.6% RH, occurring around 79.3% RH [1]. As shown in Figure 3i, the ECH sensor can maintain a high response voltage for a long time at 91.5% RH.

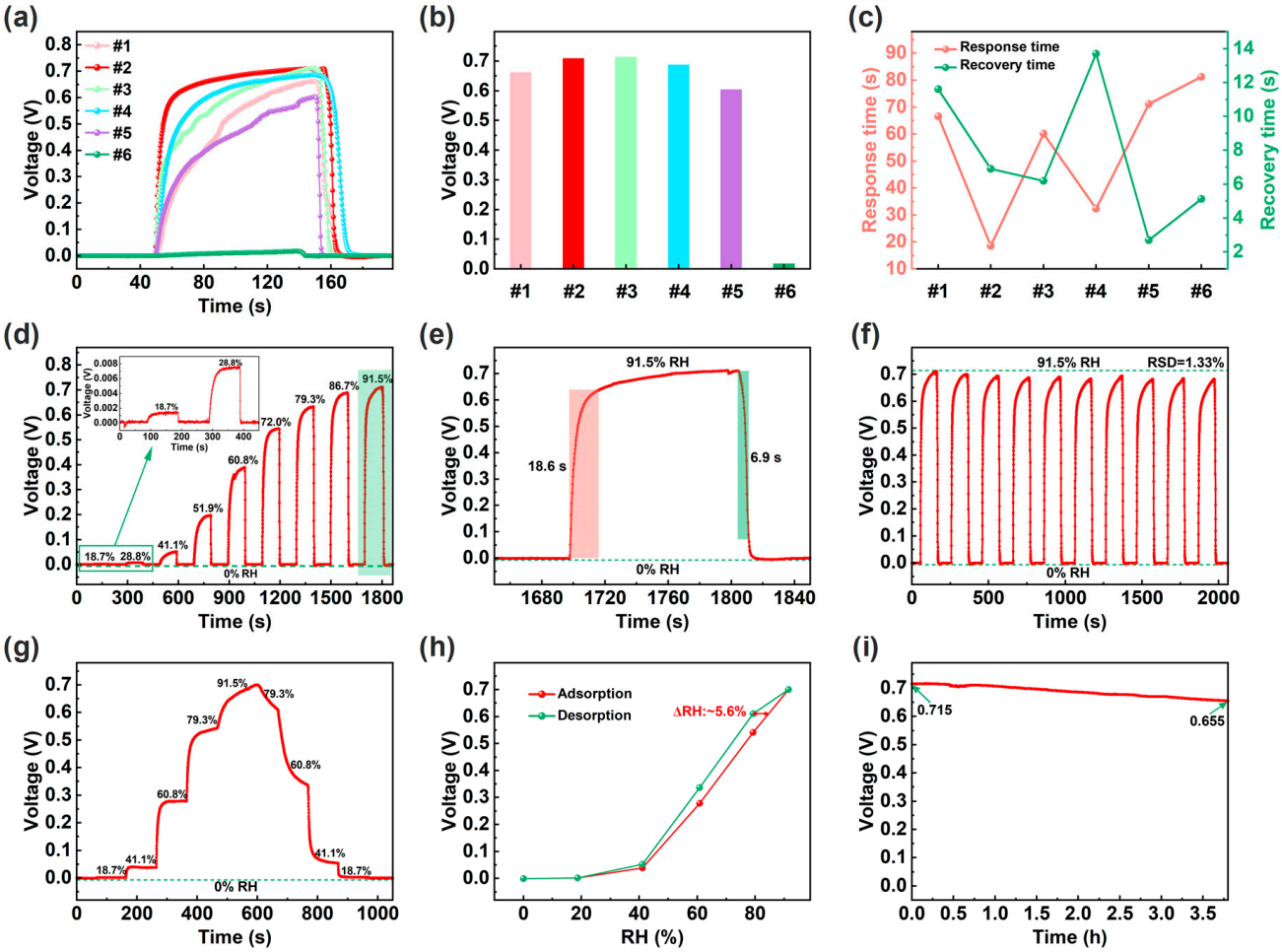


Figure 3. (**a**) Response curves of the different humidity sensors under 91.5% RH. (**b**) Response voltage values of the different humidity sensors under 91.5% RH. (**c**) Response and recovery times of the different humidity sensors under 91.5% RH. (**d**) Response and recovery curve of the optimized ECH sensor (i.e., #2) under different RHs, and the inset shows the response and recovery curve under 18.7% and 28.8% RH. (**e**) Response and recovery time curve at under 91.5% RH. (**f**) Repetitive response and recovery curves. (**g**) Response curve during water molecule adsorption and desorption processes. (**h**) Humidity hysteresis curves of the ECH sensor. (**i**) Continuous voltage output curve at 91.5% RH.

Figure 4 shows the power generation characteristics of the ECH sensor. Firstly, the ECH sensor is based on redox reactions to generate electricity and has the positive and negative electrode characteristics of battery (Figure 4a). Secondly, the load power characteristic of the ECH sensor was tested at 91.5% RH, and the circuit diagram is shown in Figure S2. As shown in Figure 4b, as the load resistance increases, the load voltage of the ECH sensor increases, while the output current decreases. Correspondingly, the maximum load power of a single ECH sensor is about 0.376 μW at 91.5% RH (Figure 4c). In addition, the charging characteristics of ECH sensors for capacitors were investigated. Although a single ECH sensor can charge different capacitors, the charging voltage value is insufficient (Figure 4d). By connecting three ECH sensors in series (Figure S3), the capacitor can obtain a higher charging voltage of about 2.2 V (Figure 4e). Correspondingly, the charged capacitor is sufficient to light up a light-emitting diode (LED) as shown in Figure 4f.

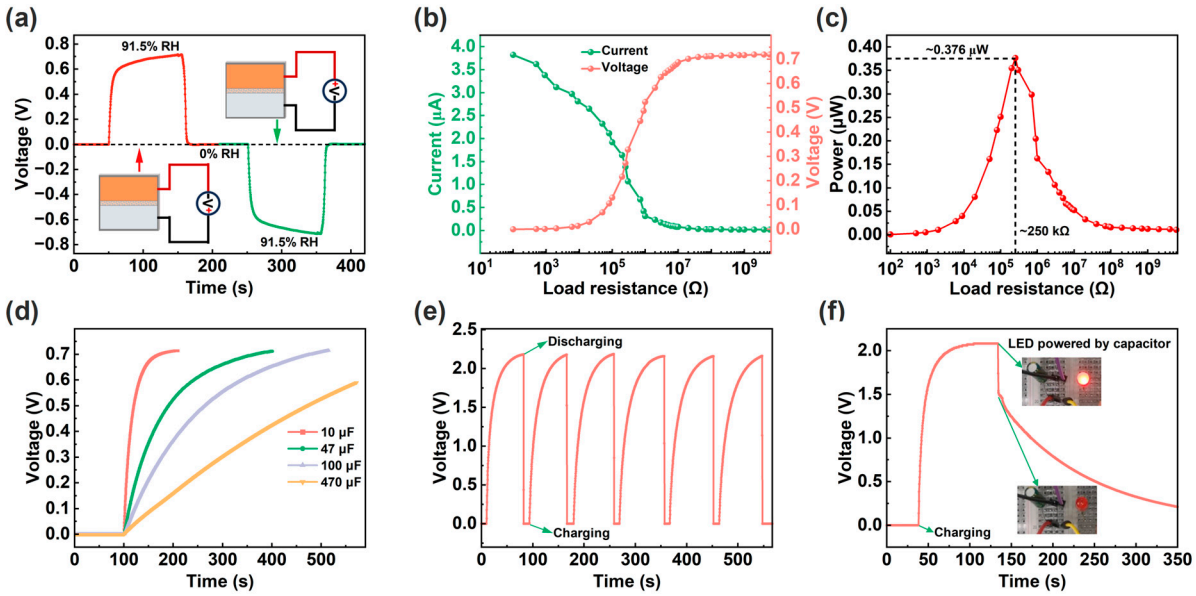


Figure 4. (**a**) Response and recovery curves of the ECH sensor after the electrodes' forward and reverse connections, and the insets show the schematic diagrams of circuit connections. (**b**) Output voltage and current curves using different load resistances. (**c**) Load power curve under different load resistances. (**d**) Charging curves. (**e**) Charging and discharging curves of three ECH sensors in series. (**f**) Charging and discharging curve, and inset shows the photo of the charged capacitor lighting up the LED.

It must be acknowledged that, compared to recently reported ECH sensors, the OH-MWCNTs/CeO_2 ECH sensor is not advanced in terms of power generation. As an attempt of traditional CeO_2 oxide in the field of ECH sensors, its humidity-sensing performance indicators can be compared. As shown in Table 1 [9–11,13,17–20,22,23], the OH-MWCNTs/CeO_2 ECH sensor balances a wide detection range, fast response/recovery speed, and high response voltage.

Table 1. Comparisons of the OH-MWCNTs/CeO_2 ECH sensor and recently reported ECH sensors.

Main Humidity-Sensing Materials	Detecting Range (RH)	Low RH Response (RH)	Response/Recovery Time (s)	Maximum Response Voltage (V)	Refs.
NaCl/paper	0%–91.5%	41.1%	109/113	0.58 (91.5% RH)	[9]
NaCl/halloysite nanotubes	0%–91.5%	10.9%	11.3/19.5	0.537 (91.5% RH)	[10]
WS_2	0%–91.5%	18.7%	8.4/5.2	0.47(91.5% RH)	[11]
sodium alginate/LiCl	0%–95%	11%	46/68	1.03 (95% RH)	[13]
polystyrene sulfonic acid/PVA/LiCl	33%–91%	33%	52.1/56.8	0.67 (91% RH)	[17]
silk nanofiber	30%–90%	30%	Not mentioned	0.346 (90% RH)	[18]
PDA-$Ti_3C_2T_x$/TEMPO-oxidized cellulose/LiCl	11%–91%	11%	13/50	0.54 (91% RH)	[19]
$MgCl_2$/CNTs	11%–97%	11%	10/46	1.07 (97% RH)	[20]
bacterial cellulose	43%–97%	43%	28.5/54.1	0.53 (97% RH)	[22]
LiCl	0%–91.5%	10.9%	36.9/38.0	0.4 (91.5% RH)	[23]
OH-MWCNTs/CeO_2	0%–91.5%	18.7%	18.6/6.9	0.711 (91.5% RH)	This work

3.3. Working Mechanisms

The performances of ECH sensors are derived from redox reactions regulated by humidity [29]. As shown in Figure 5, water molecules adsorb on the surface of OH-

MWCNTs/CeO_2 and dissociate to form H^+ (Equation (1)). Based on our previous research [14], the reduction reaction occurring at the Cu positive electrode is mainly dominated by H^+ (the positive impact of oxygen is minimal), forming H_2 (Equation (2)), while the Zn negative electrode undergoes oxidation reaction to form Zn^{2+} (Equation (3)). As humidity increases, more water molecules are adsorbed, which helps to form more H^+ and also facilitates the formation of continuous water films for conduction, thereby enhancing the redox reaction and improving the response voltage of the ECH sensor. CeO_2 itself has humidity-sensing performance. Figure 3a shows that CeO_2 ECH sensor can output a large humidity-sensing response voltage. After optimization by OH-MWCNTs, the response voltage of OH-MWCNTs/CeO_2 ECH sensor has increased and the response speed has been improved. The main reason is that OH-MWCNTs enhances the hydrophilicity of CeO_2.

$$H_2O \rightarrow H^+ + OH^- \quad (1)$$

$$2H^+ + 2e^- = H_2 \quad (2)$$

$$Zn - 2e^- = Zn^{2+} \quad (3)$$

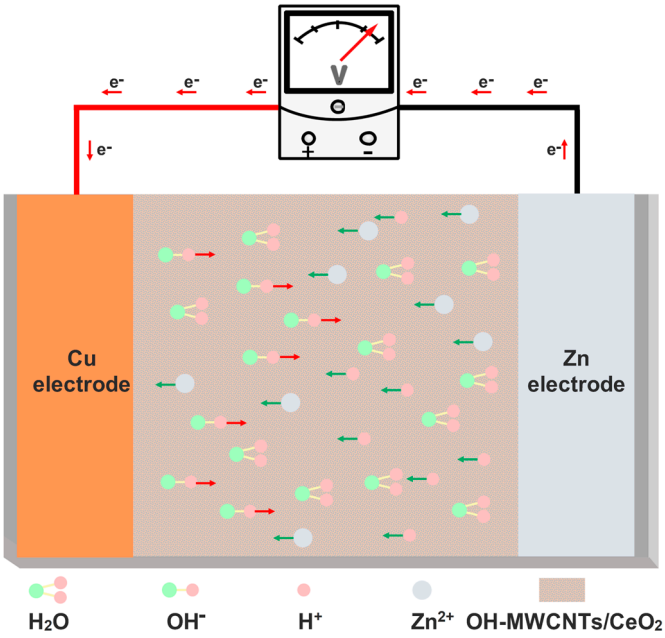


Figure 5. Schematic diagram of the working mechanism.

3.4. Applications

Compared to traditional contact switches, non-contact switches can avoid switch wear and bacterial transmission [24]. Non-contact switch function can be achieved based on human finger skin humidity and humidity sensors. As a proof of concept, we tested the potential applications of the ECH sensor. As shown in Figure 6a, when the finger approaches and moves away from the ECH sensor (distance: ~0.5 cm), the response curves of the sensor exhibit typical switching characteristics. Specifically, the different switch levels can be achieved through finger dwell time. When the finger holds for a long time, the response of the sensor increases due to the adsorption of more water molecules from the finger. In addition, humidity sensors can also achieve respiratory rate detection by utilizing the high humidity characteristics of exhaled air [10,58–61]. The ECH sensor is fixed on the mask to simulate monitoring different respiratory rates [25]. Figure 6b shows the response curves at different respiratory rates (slow, normal, and fast modes), meeting the detection requirements for different respiratory rates [10].

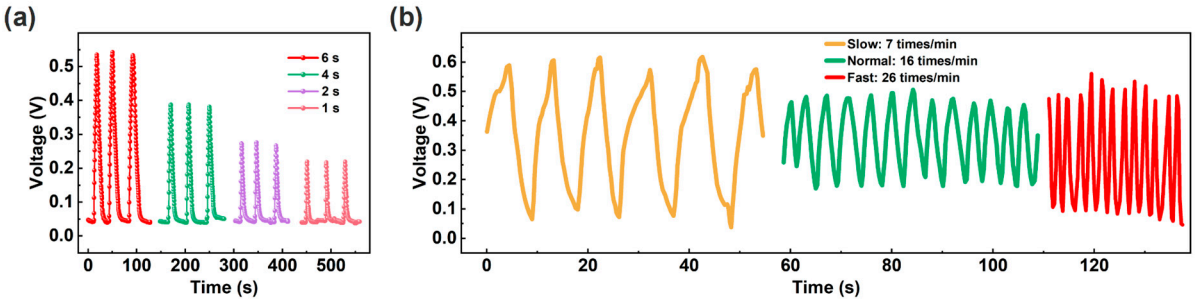


Figure 6. (**a**) Non-contact switch characteristics with different holding times of the finger. (**b**) Response curves at different respiratory rates.

4. Conclusions

This study develops a self-powered ECH sensor utilizing OH-MWCNTs-modified CeO_2 nanoparticles as the humidity-sensing materials. The research demonstrates that the incorporation of OH-MWCNTs significantly enhances the humidity-sensing performances of the CeO_2 nanoparticles. The optimized OH-MWCNTs/CeO_2 ECH sensor exhibited a wide detection range (0–91.5% RH) and rapid response/recovery times (18.6 s and 6.9 s). In addition, we validate the applications of the OH-MWCNTs/CeO_2 ECH sensor in non-contact switch and respiratory rate detection. Collectively, this work provides ideas for the application of oxides represented by CeO_2 in the field of ECH sensors.

Supplementary Materials: The following supporting information can be downloaded at: https://www.mdpi.com/article/10.3390/technologies13100467/s1, Figure S1: XPS fully scanned spectra of the OH-MWCNTs, CeO_2, and OH-MWCNTs/CeO_2; Figure S2: Schematic diagrams for measuring (a) output voltage and (b) output current with different load resistances; Figure S3. Schematic diagram for lighting the LED using the capacitance charged by the three ECH sensors in series.

Author Contributions: Conceptualization, Z.Y. and Z.D.; methodology, C.T.; validation, Z.D.; formal analysis, Y.J. and H.T.; investigation, Z.Y. and C.T.; data curation, Z.Y.; writing—original draft preparation, Z.Y.; writing—review and editing, Z.D., Y.J., and H.T.; supervision, H.T.; project administration, Y.J. and H.T.; funding acquisition, Z.D. and Z.Y. All authors have read and agreed to the published version of the manuscript.

Funding: This work is supported by the National Science Fund for Distinguished Young Scholars (Grant No. 62225106), Natural Science Foundation of China (Grant Nos. U24A20229, 62471093, and 62301114), and Sichuan Innovation Research Group Project (Grant No. 2025NSFTD0008).

Institutional Review Board Statement: Not applicable.

Informed Consent Statement: Not applicable.

Data Availability Statement: The data of our study are available upon request.

Conflicts of Interest: The authors declare no conflicts of interest.

References

1. Zu, Y.; Duan, Z.; Yuan, Z.; Jiang, Y.; Tai, H. Electrospun nanofiber-based humidity sensors: Materials, devices, and emerging applications. *J. Mater. Chem. A* **2024**, *12*, 27157–27179. [CrossRef]
2. Shi, W.; Yang, X.; Lei, L.; Lin, J.; Liang, Q.; Huang, X.; Wu, Q.; Li, W. Human respiration monitoring using humidity and temperature dual-modal sensors for temperature-insensitive humidity sensing and synchronous temperature sensing. *Sens. Actuators A Phys.* **2025**, *395*, 117008. [CrossRef]
3. Zhang, S.; Wei, C.; Li, L.; Cui, J.; Yuan, X.; Hao, D.; Wang, H. A stable and fast-response multifunctional humidity sensor based on a polyanionic liquid containing bromide ions. *Chemosensors* **2025**, *13*, 79. [CrossRef]
4. Zhang, D.; Wang, M.; Tang, M.; Song, X.; Zhang, X.; Kang, Z.; Liu, X.; Zhang, J.; Xue, Q. Recent progress of diversiform humidity sensors based on versatile nanomaterials and their prospective applications. *Nano Res.* **2022**, *16*, 11938–11958. [CrossRef]

5. Laera, A.M.; Cassano, G.; Burresi, E.; Protopapa, M.L.; Penza, M. Flexible humidity sensor based on chemically reduced graphene oxide. *Chemosensors* **2024**, *12*, 245. [CrossRef]
6. Liu, B.; Chen, Q.; Hu, J.; Zhang, Y. Amplifying electron-donor signal of the "water gate" enabled low detection ability of a field-effect transistor-based humidity sensor. *Anal. Chem.* **2025**, *97*, 2779–2785. [CrossRef] [PubMed]
7. Ngokpho, B.; Janphuang, P.; Nijpanich, S.; Chanlek, N.; Wannapaiboon, S.; Siritanon, T.; Ngamchuea, K. Halide-mediated electrochemical modification of copper phthalocyanine for humidity sensing applications. *Mater. Adv.* **2025**, *6*, 658–669. [CrossRef]
8. Lei, D.; Zhang, Q.; Liu, N.; Su, T.; Wang, L.; Ren, Z.; Zhang, Z.; Su, J.; Gao, Y. Self-powered graphene oxide humidity sensor based on potentiometric humidity transduction mechanism. *Adv. Funct. Mater.* **2021**, *32*, 2107330. [CrossRef]
9. Duan, Z.; Yuan, Z.; Jiang, Y.; Zhao, Q.; Huang, Q.; Zhang, Y.; Liu, B.; Tai, H. Power generation humidity sensor based on primary battery structure. *Chem. Eng. J.* **2022**, *446*, 136910. [CrossRef]
10. Jiang, Y.; Duan, Z.; Fan, Z.; Yao, P.; Yuan, Z.; Jiang, Y.; Cao, Y.; Tai, H. Power generation humidity sensor based on NaCl/halloysite nanotubes for respiratory patterns monitoring. *Sens. Actuator B, Chem.* **2023**, *380*, 133396. [CrossRef]
11. Zu, Y.; Hu, J.; Yang, M.; Duan, Z.; Zhang, M.; Yuan, Z.; Jiang, Y.; Tai, H. Electrochemical power generation humidity sensor based on WS_2 nanoflakes. *Sens. Actuator B, Chem.* **2024**, *405*, 135325. [CrossRef]
12. Lu, W.; Zhang, Q.; Liu, N.; Lei, D.; Ren, Z.; Yin, J.; Jia, P.; Gao, Y. Nylon fabric/GO based self-powered humidity sensor based on the Galvanic cell principle with high air permeability and rapid-response. *Small* **2023**, *20*, 2306463. [CrossRef]
13. Zhao, W.; Li, Q.; Wang, Q.; Li, Z.; Liang, J.; Wu, W. All-printed flexible self-powered humidity sensor. *Sens. Actuator B Chem.* **2025**, *440*, 137868. [CrossRef]
14. Zhang, M.; Duan, Z.; Yuan, Z.; Jiang, Y.; Tai, H. Observing mixed chemical reactions at the positive electrode in the high-performance self-powered electrochemical humidity sensor. *ACS Nano* **2024**, *18*, 34158–34170. [CrossRef] [PubMed]
15. Dou, Y.; Tang, C.; Lu, Y. Self-powered, highly sensitive, and flexible humidity sensor based on carboxymethyl cellulose for multifunctional applications. *Langmuir* **2023**, *39*, 17436–17445. [CrossRef]
16. Guo, Y.; Xi, H.; Gu, Z.; Li, M.; Li, X.; Gao, D. A self-powered PVA-based flexible humidity sensor with humidity-related voltage output for multifunctional applications. *Colloids Surf. A* **2023**, *658*, 130700. [CrossRef]
17. Zhang, R.; Chen, X.; Wan, Z.; Yin, M.; Ma, L.; Xiao, X. Moisture electricity generation based self-powered humidity sensor for smart agriculture. *Mater. Today Chem.* **2024**, *42*, 102416. [CrossRef]
18. Wang, Z.; Yi, N.; Zheng, Z.; Zhou, J.; Zhou, P.; Zheng, C.; Chen, H.; Shen, G.; Weng, M. Self-powered and degradable humidity sensors based on silk nanofibers and its wearable and human-machine interaction applications. *Chem. Eng. J.* **2024**, *497*, 154443. [CrossRef]
19. Han, M.; Shen, W.; Corriou, J.P. Polydopamine-modified MXene/cellulose nanofibers composite film for self-powered humidity sensing and humidity actuating. *Nano Energy* **2024**, *123*, 109445. [CrossRef]
20. Eryanto, G.; Tseng, S.F. Self-powered paper-based humidity sensors with $MgCl_2$/CNTs composites. *Sens. Actuators A Phys.* **2024**, *376*, 115606. [CrossRef]
21. Tseng, S.F.; Chiu, L.Y.; Hsu, S.H.; Kuo, C.C. High performance flexible and self-powered humidity sensors based on LiCl/LIPG composites. *Sens. Actuator B Chem.* **2025**, *422*, 136569. [CrossRef]
22. Wu, H.; Jin, F.; Ge, H.-L.; Wu, Q.; Wang, Y.; Gao, F. Covalently modified nanocellulose materials: Enhanced performance and stability for self-powered and impedance humidity sensors. *Colloids Surf. A* **2025**, *716*, 136681. [CrossRef]
23. Zhao, Q.; Duan, Z.; Wu, Y.; Liu, B.; Yuan, Z.; Jiang, Y.; Tai, H. Facile primary battery-based humidity sensor for multifunctional application. *Sens. Actuator B Chem.* **2022**, *370*, 132369. [CrossRef]
24. Li, S.; Zhang, Y.; Liang, X.; Wang, H.; Lu, H.; Zhu, M.; Wang, H.; Zhang, M.; Qiu, X.; Song, Y.; et al. Humidity-sensitive chemoelectric flexible sensors based on metal-air redox reaction for health management. *Nat. Commun.* **2022**, *13*, 5416. [CrossRef]
25. Hu, J.; Duan, Z.; Tan, C.; Wang, Y.; Yuan, Z.; Jiang, Y.; Tai, H. Self-powered electrochemical humidity sensor based on Cu/(cellulose nanocrystals/NaCl)/Zn structure for respiratory rate detection. *Inorg. Chem. Commun.* **2025**, *180*, 114994. [CrossRef]
26. Cao, L.C.T.; Hakim, L.; Nagao, Y.; Boonruang, S.; Tseng, S.F.; Hsu, S.H. Self-powered humidity sensor based on porous $Ti_3C_2T_x$ MXene: High sensitivity and fast response for real-world applications. *Chem. Eng. J.* **2025**, *523*, 168345. [CrossRef]
27. Huang, Z.; Yao, L.; Lin, S.; Wei, F. Self-powered flexible humidity sensors based on ceramic fiber paper. *J. Alloys Compd.* **2025**, *1040*, 183470. [CrossRef]
28. Liao, K.; Wang, F.; Shen, Q.; Liu, Y.; Mei, Z.; Wang, H.; Zhang, S.; Ma, S.; Wang, L. Advances in humidity sensors based on Self-Powered technology. *Chem. Eng. J.* **2025**, *505*, 159480. [CrossRef]
29. Duan, Z.; Zhang, M.; Jiang, Y.; Yuan, Z.; Tai, H. Emerging electrochemical humidity sensors for zero power consumption and self-powered humidity detection: A perspective. *J. Mater. Chem. A* **2024**, *12*, 14975–14985. [CrossRef]
30. Blank, T.A.; Eksperiandova, L.P.; Belikov, K.N. Recent trends of ceramic humidity sensors development: A review. *Sens. Actuator B Chem.* **2016**, *228*, 416–442. [CrossRef]

31. Pascariu, P.; Tudorache, F.; Romanitan, C.; Serban, A.B.; Koudoumas, E. 1% lanthanide-doped ZnO nanostructures as a versatile approach for state-of-the-art capacitive and resistive humidity sensors. *Ceram. Int.* **2025**, *51*, 17090–17100. [CrossRef]
32. Zahoor, M.T.; Khan, G.A.; Nawaz, M.B.; Farouk, S.; Imran, Z.; Ahmed, W. Rapid dielectrophoresis-assisted deposition of highly concentrated ZnO nanowires for enhanced performance of humidity sensors. *Sens. Actuators A Phys.* **2023**, *362*, 114651. [CrossRef]
33. Zhang, H.; Zhang, H.; Chen, C.; Zhang, L.; Ma, X.; Li, X.; Wang, J. Preparation of silver nanoparticles modified SnO_2 humidity sensor for tobacco storage environment detection. *Sens. Actuator B Chem.* **2024**, *409*, 135612. [CrossRef]
34. Kumar, A.; Kumari, P.; Kumar, M.S.; Gupta, G.; Shivagan, D.D.; Bapna, K. SnO_2 nanostructured thin film as humidity sensor and its application in breath monitoring. *Ceram. Int.* **2023**, *49*, 24911–24921. [CrossRef]
35. Lv, X.; Feng, C.; Lin, T. Enhanced humidity sensing properties of interstitial B-doped TiO_2 nanofibers. *Sens. Actuators A Phys.* **2023**, *358*, 114412. [CrossRef]
36. Yu, Z.; Li, J.; Zhang, Q.; Xiang, P.; Lei, J. Laser-induced in situ synthesis and assembly of nano-cotton TiO_2 humidity sensors with high sensitivity and fast response for real-time respiratory monitoring. *Small Struct.* **2025**, *6*, 2400593. [CrossRef]
37. Manikandan, M.; Tippo, P.; Singjai, P.; Thongpan, W.; Jumrus, N.; Kumpika, T.; Panthawan, A.; Jhuntama, N.; Thongsuwan, W.; Sroila, W.; et al. Facile design of interdigitated electrode (IDE) based Co_3O_4 resistive type humidity sensor by a novel spark discharge method. *Inorg. Chem. Commun.* **2025**, *177*, 114431. [CrossRef]
38. Taha, W.M.; Morsy, M.; Nada, N.A.; Ibrahim, M. Studying the humidity sensing behavior of MWCNTs boosted with Co_3O_4 nanorods. *Diamond Relat. Mater.* **2022**, *121*, 108754. [CrossRef]
39. Yu, H.; Wang, C.; Meng, F.; Xiao, J.; Liang, J.; Kim, H.; Bae, S.; Zou, D.; Kim, E.S.; Kim, N.Y.; et al. Microwave humidity sensor based on carbon dots-decorated MOF-derived porous Co_3O_4 for breath monitoring and finger moisture detection. *Carbon* **2021**, *183*, 578–589. [CrossRef]
40. Manikandan, V.; Petrila, I.; Vigneselvan, S.; Mirzaei, A.; Mane, R.S.; Kim, S.S.; Chandrasekaran, J. Enhanced humidity sensing properties of Fe-doped CeO_2 nanoparticles. *J. Mater. Sci. Mater. Electron.* **2020**, *31*, 8815–8824. [CrossRef]
41. Li, H.; Liu, Y.; Zhang, X.; Guo, C.; Zhang, H.; Zhao, X.; Huo, L.; Dong, X.; Huang, C.; Cheng, X.; et al. Preparation of nest-like CeO_2 humidity sensing material and its application in eye strain monitoring. *Sens. Actuator B Chem.* **2024**, *415*, 135985. [CrossRef]
42. Jakhar, S.; Sheoran, G.; Rohilla, B.; Malik, P.; Duhan, S. Structural and sensing insights of CeO_2/KIT-6 for humidity detection applications. *Mater. Chem. Phys.* **2025**, *343*, 131056. [CrossRef]
43. Liu, Y.; Huang, H.; Wang, L.; Cai, D.; Liu, B.; Wang, D.; Li, Q.; Wang, T. Electrospun CeO_2 nanoparticles/PVP nanofibers based high-frequency surface acoustic wave humidity sensor. *Sens. Actuator B Chem.* **2016**, *223*, 730–737. [CrossRef]
44. Geeta, B.; Bikshalu, K.; Rajendar, V.; Rao, K.V. Nanostructured conducting polyaniline (NSPANI)/CeO_2 nanocomposites for humidity sensors application. *J. Mater. Sci. Mater. Electron.* **2017**, *29*, 374–381. [CrossRef]
45. Chani, M.T.S. Fabrication and characterization of chitosan-CeO_2-CdO nanocomposite based impedimetric humidity sensors. *Int. J. Biol. Macromol.* **2022**, *194*, 377–383. [CrossRef]
46. Gong, L.; Wang, X.; Zhang, D.; Ma, X.; Yu, S. Flexible wearable humidity sensor based on cerium oxide/graphitic carbon nitride nanocomposite self-powered by motion-driven alternator and its application for human physiological detection. *J. Mater. Chem. A* **2021**, *9*, 5619–5629. [CrossRef]
47. Xie, W.; Liu, B.; Xiao, S.; Li, H.; Wang, Y.; Cai, D.; Wang, D.; Wang, L.; Liu, Y.; Li, Q.; et al. High performance humidity sensors based on CeO_2 nanoparticles. *Sens. Actuator B Chem.* **2015**, *215*, 125–132. [CrossRef]
48. Zhang, P.; Zhang, L.; Xu, H.; Xing, Y.; Chen, J.; Bie, L. Ultrathin CeO_2 nanosheets as bifunctional sensing materials for humidity and formaldehyde detection. *Rare Met.* **2020**, *40*, 1614–1621. [CrossRef]
49. Cheng, Y.; Jiang, B.; Chaemchuen, S.; Verpoort, F.; Kou, Z. Advances and challenges in designing MXene quantum dots for sensors. *Carbon Neutralization* **2023**, *2*, 213–234. [CrossRef]
50. Dai, Z.; Lei, M.; Ding, S.; Zhou, Q.; Ji, B.; Wang, M.; Zhou, B. Durable superhydrophobic surface in wearable sensors: From nature to application. *Exploration* **2023**, *4*, 20230046. [CrossRef]
51. Zhang, Y.; Zhang, G.; Dong, Y.; Wu, Y.; Yu, L.; Bai, Y. Interfacial modulation of polydopamine-reduced graphene oxide for achieving highly conductive and strong graphene/cotton composite yarn toward smart wearable devices. *Adv. Fiber Mater.* **2024**, *6*, 1798–1812. [CrossRef]
52. Rajavel, K.; Lalitha, M.; Radhakrishnan, J.K.; Senthilkumar, L.; Rajendra Kumar, R.T. Multiwalled carbon nanotube oxygen sensor: Enhanced oxygen sensitivity at room temperature and mechanism of sensing. *ACS Appl. Mater. Interfaces* **2015**, *7*, 23857–23865. [CrossRef]
53. Nazir, M.A.; Najam, T.; Ullah, S.; Hossain, I.; Javed, M.S.; Naseer, M.; Rehman, A.; Shah, S.S.A. Recent advances in MXene nanomaterials: Fundamentals to applications in environment sector. *EcoEnergy* **2024**, *2*, 505–548. [CrossRef]
54. Duan, Z.; Jiang, Y.; Yan, M.; Wang, S.; Yuan, Z.; Zhao, Q.; Sun, P.; Xie, G.; Du, X.; Tai, H. Facile, flexible, cost-saving, and environment-friendly paper-based humidity sensor for multifunctional applications. *ACS Appl. Mater. Interfaces* **2019**, *11*, 21840–21849. [CrossRef]

55. Futaba, D.N.; Yamada, T.; Kobashi, K.; Yumura, M.; Hata, K. Macroscopic wall number analysis of single-walled, double-walled, and few-walled carbon nanotubes by X-ray diffraction. *J. Am. Chem. Soc.* **2011**, *133*, 5716–5719. [CrossRef]
56. Singh, D.K.; Iyer, P.K.; Giri, P.K. Diameter dependence of interwall separation and strain in multiwalled carbon nanotubes probed by X-ray diffraction and Raman scattering studies. *Diamond Relat. Mater.* **2010**, *19*, 1281–1288. [CrossRef]
57. Guo, C.; Xin, Y.; Liu, Y.; Na, B.; Meng, W.; Zhang, X.; Cheng, X.; Huo, L.; Wang, T.; Xu, Y. Noncontact sensing for water area scanning identification based on Ho_2O_3/GO humidity sensor. *Sens. Actuator B Chem.* **2023**, *385*, 133683. [CrossRef]
58. Zhao, R.; Xie, D.; Qing, S.; Zhu, B.; Shen, W.; Wang, L.; Meng, X.; Pang, J. Cellulose acetate and reduced graphene oxide (rGO)-based flexible humidity sensor for monitoring human respiration. *Sens. Actuator B Chem.* **2025**, *429*, 137291. [CrossRef]
59. Zhang, Z.; Li, J.; Chen, H.; Wang, H.; Luo, Y.; Si, R.; Xie, R.; Tao, K.; Yang, B.R.; Zhang, D.; et al. Scalable fabrication of uniform fast-response humidity field sensing array for respiration recognition and contactless human-machine interaction. *Adv. Funct. Mater.* **2025**, *35*, 2502583. [CrossRef]
60. You, Q.; Gao, C.; Pan, M.; Wei, T.; Shen, W.; Yao, X.; Yang, X.; Yang, Z.; Li, Y.; Li, X.; et al. A seamlessly integrated device of wireless energy storage and humidity sensing for human-machine interaction of respiration. *Small* **2025**, *21*, 2501122. [CrossRef] [PubMed]
61. Mandal, S.; Mantilla, H.M.; Loganathan, K.; Faber, H.; Sharma, A.; Gedda, M.; Yengel, E.; Goswami, D.K.; Heeney, M.; Anthopoulos, T.D. Ultra-fast moisture sensor for respiratory cycle monitoring and non-contact sensing applications. *Adv. Mater.* **2025**, *37*, 2414005. [CrossRef] [PubMed]

Disclaimer/Publisher's Note: The statements, opinions and data contained in all publications are solely those of the individual author(s) and contributor(s) and not of MDPI and/or the editor(s). MDPI and/or the editor(s) disclaim responsibility for any injury to people or property resulting from any ideas, methods, instructions or products referred to in the content.